Brazilian Journal
of Chemical
Engineering

ISSN 0104-6632
Printed in Brazil
www.abeq.org.br/bjche

Vol. 36, No. 04, pp. 1631 - 1643, October - December, 2019
dx.doi.org/10.1590/0104-6632.20190364s20180258

CHEMICAL REGENERATION OF BONE CHAR ASSOCIATED WITH A CONTINUOUS SYSTEM FOR DEFLUORIDATION OF WATER

Elbert M. Nigri[1*], André L. A. Santos[1], Amit Bhatnagar[2] and Sônia D. F. Rocha[1]

[1] Universidade Federal de Minas Gerais, Departamento de Engenharia de Minas, Belo Horizonte, MG, Brasil.
E-mail: elbertnigri@gmail.com - ORCID: 0000-0001-9801-3157; E-mail: asantos@demin.ufmg.br - ORCID: 0000-0001-6764-2014;
E-mail: sdrocha@demin.ufmg.br - ORCID: 0000-0002-4775-6329
[2] University of Eastern Finland, Department of Environmental and Biological Sciences, Kuopio, Finland. E-mail: amit.bhatnagar@uef.fi -
ORCID: 0000-0002-3565-9943

(Submitted: January 13, 2019 ; Revised: March 1, 2019 ; Accepted: May 5, 2019)

Abstract - Sources of fluoride contaminated water are found around the world and their treatment is required before human consumption. This paper contributes to advances in the use of bone-char as an adsorbent for fluoride, associating steps of chemical regeneration and fluoride adsorption in continuous systems, thereby making feasible the multiple use of the adsorbent. Following the development of low cost treatment of water defluoridation in a fixed bed column, using bone-char, regeneration was carried out with NaOH (0.5 mol/L) solution in subsequent adsorption/desorption cycles. The continuous system was modeled applying Thomas, Yoon-Nelson, Adams-Bohart, Wolborska and Yan models, and the Yan model showed the best adjustment. The adsorption capacity of 6.28 mg/g was obtained from the breakthrough curve. Chemical regeneration of bone-char was feasible, and a reduction in adsorption capacity of 30% was observed only after five adsorption/desorption cycles.
Keywords: Bone-char; Chemical regeneration; Fluoride removal; Column modeling; Adsorption/desorption's cycles.

INTRODUCTION

Fluoride is an essential element for human health that in lower concentrations, between 0.4 and 1.0 mg/L, prevents dental diseases (Ghorai and Pant, 2004; WHO, 1996). The World Health Organization (WHO) recommends the value of 1.5 mg/L as the safe concentration of fluoride in water for human consumption (WHO, 1996). Prolonged intake of water containing fluoride above 2 mg/L may cause dental fluorosis and in extreme cases, serious diseases such as skeletal fluorosis, osteoporosis, arthritis, male infertility, Alzheimer's disease, and liver, kidney or parathyroid lesions may occur (Harrison, 2005; Tripathy et al., 2006; Nur et al., 2014; Xiong et al., 2007).

Water contaminated by fluoride has been found naturally and causes serious environmental and health problems in several parts of the world (Nur et al., 2014). At least 25 countries around the world have been reported to be affected due to high fluoride concentrations in groundwaters, above the World Health Organization limit (Davila-Rodriguez et al., 2012; Gupta et al., 2007). Diseases due to fluoride contaminated water ingestion in many cities of the world are widely described in the literature. The occurrence of fluorosis is reported in the Brazilian states of São Paulo, Paraná, Santa Catarina, Rio de Janeiro and Minas Gerais (Santiago and Silva, 2009). Meneasse et al. (2002) pointed out high fluoride concentrations in São Francisco city in the northern part of Minas Gerais State, in the range of 1.17 to 5.2 mg/L.

Several methods have been used to reduce the fluoride content in water, to make it suitable for human

* Corresponding author: Elbert M. Nigri - E-mail: elbertnigri@gmail.com

consumption (Agarwal et al., 2003). Among them, adsorption (Medellin-Castillo et al., 2007), chemical precipitation (Benefield et al., 1982), ion exchange (Kunin, 1990), reverse osmosis (Colla et al., 2016), electrodialysis (Gwala et al., 2011) and nanofiltration (Simons, 1993) are the most common methods.

Compared to other techniques, adsorption stands out if its simple operating system is coupled with low cost adsorbents, which makes the application feasible for communities of limited financial resources (Bhatnagar et al., 2011; Tripathy et al., 2006; Vocciante et al., 2014). Several adsorbents have been studied and applied for fluoride uptake from contaminated waters (Bhatnagar et al., 2011; Loganathan et al., 2013). One of them is the bone char, which presents high fluoride removal capacity (Abe et al., 2004; Leyva-Ramos et al., 2010; Medellin-Castillo et al., 2007).

Bone char is an association of carbonaceous and inorganic materials containing from 70 to 76% of calcium phosphate, as hydroxyapatite (HAP, $Ca_{10}(PO_4)_6(OH)_2$) that has been effectively used to reduce the content of fluoride in water and wastewater (Wilson et al., 2003). In addition, characteristics such as specific surface area and its positively charged surface below pH 8.4 promote better adsorption capacity for bone char than that observed for conventional coals (Brunson and Sabatini, 2009; Medellin-Castillo et al., 2007).

Although the mechanisms and studies of bone char application for fluoride and other elements removal have been developed, efforts on spent adsorbent regeneration or its destination have not been adequately studied. There are only a few studies that have looked into these aspects and this may hinder industrial applications. Regeneration methods are necessary to evaluate the application of bone char, its lifetime, which can reduce the cost of the process and decrease the amount of undesired wastes (Sheintuch and Matatov-Metal, 1999).

Thermal and chemical regeneration of fluoride saturated bone char have been studied recently (Feng et al., 2012; Kaseva, 2006; Nasr et al., 2011). In the study of Medellin-Castilho et al. (2007), the elevation of pH above 12 provides desorption of fluoride present in bone char. This is because, with increasing pH, the fluoride ion inserted in the hydroxyapatite structure contained in bone char is released into solution, exchanged by the hydroxide ion, an ionic substitution mechanism already described in other studies (Kaseva, 2006; Medellin-Castilho et al., 2014; Sternitzke et al., 2012; Sundaram et al., 2008). Kanyora et al. (2014) verified that the use of NaOH solutions presented better results in the regeneration of bone char when compared to other compounds. An actual application performed by the Catholic Diocese of Nakuru Water Quality (Jacobsen and Müller, 2007) using NaOH presented satisfactory results in bone char regeneration.

However, these processes still require knowledge about the reduction in the adsorption capacity through a regenerative process and the extent of regeneration in successive cycles of adsorption-regeneration.

In order to recover the bone char adsorption capacity, the mechanisms of fluoride uptake by the bone char must be well known. The hydroxyapatite contained in the bone char exchanges OH^- groups for F^-, being one of the advantages of bone char compared to conventional activated coals applied to water treatment (Kaseva, 2006). The exchange of groups may be represented by equation 1.

$$Ca_{10}(PO_4)_6(OH)_{2(s)} + 2F^-_{(aq)} \rightarrow Ca_{10}(PO_4)_6F_{2(s)} + 2OH^-_{(aq)} \quad (1)$$

Fluoride removal can also occur in carbonous structures and through calcium fluoride (CaF_2) precipitation (Sternitzke et al., 2012). However, Medellin-Castilho et al. (2014) highlight that the fluoride removal by bone char is mainly associated with hydroxyapatite. They suggested that fluoride uptake occurs through complex formation on phosphate (≡P-OH) and hydroxyl (≡Ca-OH) sites and that CaF_2 precipitation is possible, since calcium ions are partially dissolved from bone char (hydroxyapatite and calcite) and may supersaturate the water if the calcium fluoride solubility is overpassed. Furthermore, they concluded that the removal of fluoride in the bone char mainly occurs due to electrostatic interactions between the adsorbent surface charges and adsorbate ions and not through ionic interchange, as proposed by Kaseva (2016). Below a pH of point of zero charge, the protonation of sites is favored, forming positively charged complexes on the bone char surface (equations 2 and 3) that interact with fluoride ions. Through all these removal mechanisms, the term sorption is better applied instead of adsorption since adsorption, precipitation and also complexation mechanisms are involved.

$$\equiv P-OH + H^+ \rightarrow \equiv P-OH_2^+ \quad (2)$$

$$\equiv Ca-OH + H^+ \rightarrow \equiv Ca-OH_2^+ \quad (3)$$

This paper aims to present the advances in knowledge of defluoridation by bone char integrating steps of sorbent regeneration and fluoride removal in continuous systems. The life time or regenerative cycles supported by bone char are determined.

MATERIALS AND METHODS

Bone char supply

Bone char was supplied by Bonechar Carvão Ativado do Brasil, a Brazilian company that produces

bone char from bovine's bones pyrolyzed at 750°C. Bone char with particle sizes between 1.0 to 1.6 mm was washed with 0.1 mol/L of HCl solution in a ratio of 40 g/L for 1 h at constant stirring. Further, the solid was washed with distilled water three times and dried at 50°C for 24 h based on previous methodology adopted by Nigri et al. (2017a).

Fluoride solutions and chemical analysis

A stock solution of 100 mg/L of fluoride was prepared through dissolving a weighed quantity of NaF (A.G. Merck) in distilled water. Buffering solutions at a predetermined concentration and fluoride solution for continuous experiments were prepared from the dilution of stock solution. Fluoride concentration in solution was measured with a specific ion electrode Thermo Scientific Orion 9609BNWP in TISABII solution prepared by dissolving DCYTA monohydrate (A.G. MACRON) and NaCl (A.G. Fisher Scientific) in a mixture of distilled water and acetic acid (A.G. Fisher Scientific). The pH of TISABII solution was raised to 5.5 with NaOH solution (APHA, 2012).

Column set up and modeling

Experiments in fixed bed column were performed using a polycarbonate column of 2.3 cm of internal diameter and 13 cm length with an empty bed volume of 54.01 cm^3. At the base and the top of the column, glass beads, followed by glass wool, were placed to enhance the solution distribution and keep the media intact. The column was packed with 30.36 g of bone char and the experiments were carried out using 10 mg/L fluoride solution previously prepared with NaF. The solution was pumped through the column from the bottom to the top at 5 mL/min using a variable-flow peristaltic pump (Spetec Perimax 121). Columns were packed with wet bone char to ensure consistent packing.

Samples were collected periodically at each 180 min for pH and fluoride residual concentration when the relative concentration reached the condition $C_{effluent} = 0.9\ C_{influent}$. The breakthrough curve obtained in this experiment was evaluated through the models of Thomas, Yoon-Nelson, Adams-Bohart, Wolborska and Yan, and the design of the column was carried out in accordance with the best model. The *OriginPro8* software was used to obtain the parameters of the breakthrough curve and the fit of the breakthrough curve models, which were inserted in the software.

Regeneration experiments

The same set up employed for column modeling was applied for regeneration experiments. Bone char was loaded with fluoride until its concentration at the end of the column presented a residual concentration of 1.5 mg/L, a maximum value permitted by the WHO for human consumption. The time to get to this condition was estimated from previous tests and this value was considered in the subsequent adsorption experiment associated with the regeneration step.

Regeneration of bone char was carried out in a packed column by pumping 2 L of NaOH 0.5 mol/L from the top to the bottom at a flow rate of 5 mL/min. This sodium hydroxide concentration was the same as applied by Nigri et al. (2017a) and it is in agreement with recent studies by Kanyora et al. (2015) and Kanyora et al. (2014). Fluoride concentration was monitored during the regeneration cycle until the concentration of residual fluoride stabilized (390 min). After that, distilled water was pumped throughout the column to wash the remaining NaOH until the pH was stabilized. Then, another adsorption cycle began by pumping the fluoride solution at 10 mg/L. Details of the bone char characterization and adsorption-regeneration process in batch and continuous operation can be found in Nigri et al. (2017a) and Nigri et al. (2017b).

Sorbent characterization techniques

The functional groups present on the surface of bone char were identified by Fourier-Transform Infrared Spectroscopy (FTIR) (Bruker Alpha, attenuated total reflectance - ATR, with a diffuse reflectance accessory - DRIFT) in the solid form. The particles were previously crushed for analysis. For measurement of specific surface area and porosity, the data were obtained using a QUANTACHROME device model NOVA-1000, adsorption surface area analyzer and pore size distribution from adsorption condensation of nitrogen gas (N_2). Zeta potential measurements were performed using a ZM3-D-G meter, Zeta Meter system 3.0+, with direct video imaging.

The morphology and the chemical composition of the bone char were assessed by scanning electron microscopy (SEM) and energy-dispersive x-ray spectroscopy (EDS) microanalysis (Scanning Electron Microscope Model 6360LV Dispersive Spectrometer coupled to an in-EDS wavelength).

RESULTS AND DISCUSSION

Bone char characterization

Table 1 shows the specific surface area and porosity from fresh bone char and saturated bone char. The value of the surface area and pore volume for bone char are similar to values highlighted by other studies with bone char (Cheung et al., 2002; Medellin-Castillo et al., 2007; Rojas-Mayorga et al., 2013; Walker and Weatherley, 2001).

After the adsorption process it is possible to observe a reduction in the specific surface area and porosity, which can be caused by fluoride presence on the surface of bone char. The average pore diameter obtained is compatible with a mesoporous structure according to IUPAC (20 to 500 Å) (Burwell, 1976).

Table 1. Textural characteristics of the fresh bone char and saturated bone char.

Characteristic	Fresh bone char	Saturated bone char
Surface area (m^2/g)	119.3	111.5
Total pore volume (cm^3/g)	0.304	0.287
Average pore radius (Å)	50.98	51.46
Pore volume (cm^3/g)	0.285	0.270
Pore area (m^2/g)	95.43	90.82

The surface charge is an important characteristic to explain the ion sorption onto bone char and comes from the interactions between the ions present in the solution and the surface functionalities. It also depends on ion type, surface properties and solution pH (Medellin-Castillo et al., 2007; Nigri et al., 2017a). Fig.1 shows the zeta potential for the fresh bone char.

The surface is positively charged when the pH of the solution is below the isoelectric point and negatively charged above the isoelectric point. As shown in Fig. 1, the pH_{PZC} was, approximately, 8.1 which is similar to the value of 8.4 found by Medellin-Castillo et al. (2014).

Hence, the solution pH directly affects the fluoride sorption, whereas in pH solutions below the pH_{PZC}, the F^- anions are attracted by the positively charged surface of the bone char, caused by the protonation of the hydroxyapatite hydroxyl groups, thus favoring the F^- accumulation onto the surface (Nigri et al, 2016a).

The FTIR spectra in Figure 2 show the absorption bands corresponding to the structural composition of the fresh and fluoride saturated bone char samples. According to Rojas-Mayorga et al. (2015), the groups corresponding to the bands in Fig. 2A are: CC (1455 cm^{-1}), PO_4^{3-} (1409 and 600 cm^{-1}), CO_3^{2-} (870 and 1409 cm^{-1}) and Ca (566 cm^{-1}) and, according to Thompson et al. (2009), CO_3^{2-} (870, 1409 cm^{-1}), PO_4^{3-} (566, 600 and 1035 cm^{-1}). According to Dimović et al. (2009), the bands at 1090, 960, 600, 566 cm^{-1} are assigned to the PO_4^{3-} group and Tianyuan et al. (2011) also states

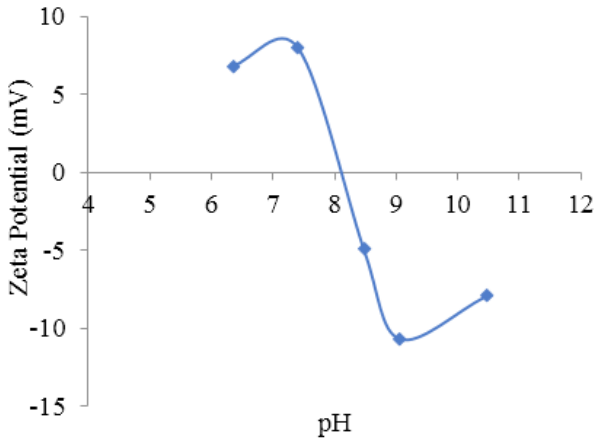

Figure 1. Zeta Potential for fresh bone char.

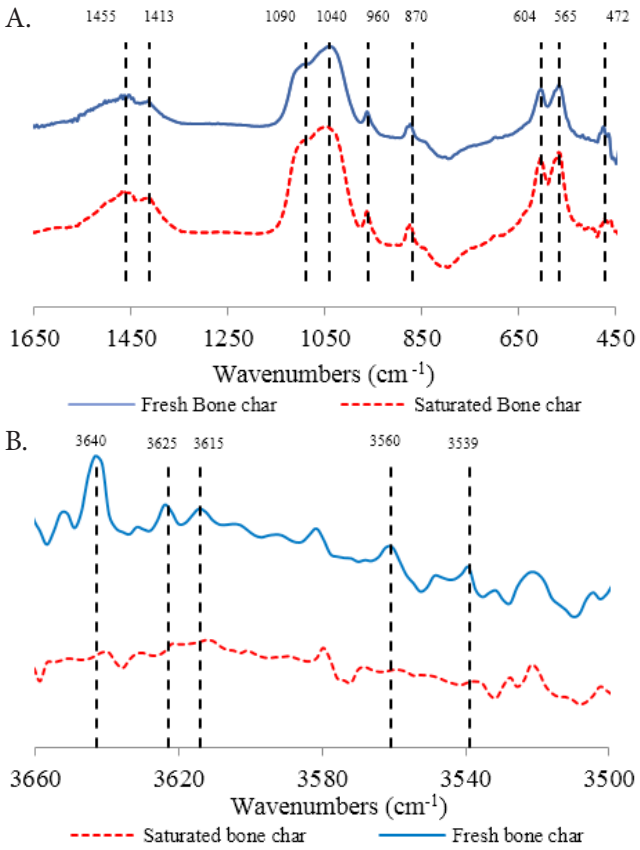

Figure 2. FTIR analysis for fresh and saturated bone char with fluoride samples after the fifth cycle of adsorption.

bands of 1030 and 469 cm^{-1} as due to the PO_4^{3-} group, present in their bone char sample. Nigri et al. (2017b) also identified bands at 566, 600 cm^{-1} as typical of hydroxyapatite - HAP.

These FTIR spectra (Fig. 2B) of the fresh bone char and saturated bone char, even after the fifth adsorption cycle did not exhibit many differences. However, after the saturation and regeneration process, it is possible to observe that the bands 3539, 3560, 3615, 3625 and 3640 cm^{-1} are present only in the fresh bone char sample. The bands from 3000 to 3600 cm^{-1}, correspond to OH groups, and the bands between 3640 and 3610 correspond to free OH group, which suggested the occurrence of the ion exchange process between F^- and OH^- groups from doped bone char (Nigri et al. 2017b). A similar result was obtained by Rojas Mayorga et al. (2015).

SEM/EDS analysis was performed to assess the particle morphology. Various irregularities and porosity variations and discrepancies between grains may be observed (Fig. 3). The EDS (Table 2) analysis showed elevated levels of phosphorus and calcium, owing to the composition of the hydroxyapatite present in the bone char as was already observed by Wilson et al. (2003) and Medellin-Castillo et al. (2007).

Through Table 2 it is also possible to observe that the molar ratio Ca/P of the raw bone char was

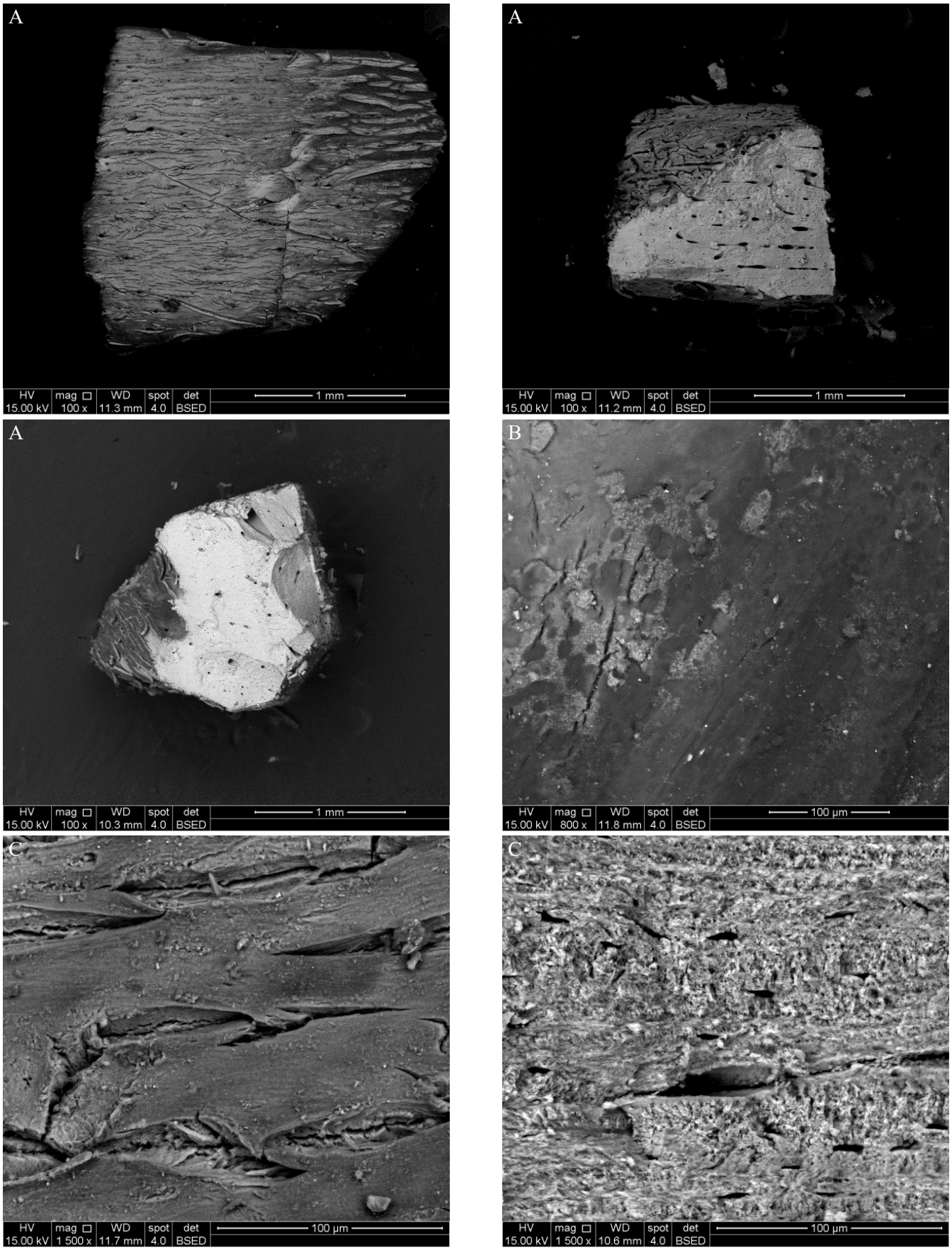

Figure 3. Back scattered electron images of SEM analysis of raw bone with magnification of 100X (A), 800X (B) and 1500X (C).

Table 2. Energy Dispersive Spectrometry (EDS) made on raw bone char.

Element	Wt%	At%	Z	A	F
O	31.58	51.18	1.0543	0.1674	1.0001
F	0.00	0.00	0.9897	0.1864	1.0004
Na	0.35	0.39	0.9834	0.4505	1.0019
Mg	0.56	0.59	1.0070	0.6030	1.0039
Al	0.38	0.37	0.9776	0.7306	1.0078
P	21.50	18.00	0.9694	0.8962	1.0091
Ca	45.31	29.31	0.9718	0.9703	1.0001
Fe	0.32	0.15	0.8772	0.9746	1.0000
Total	100.00	100.00			

Z: Atomic Number Effect; A: X-Ray Absorption Effect; F: X-Ray Fluorescence Effect.

1.63, approximately the value obtained for pure hydroxyapatite ([Ca/P] = 1.67) (Krzesińska and Majewska 2015), which confirms the predominance of HAP in the adsorbent composition.

Continuous column adsorption studies

Breakthrough curve and adsorption capacities

According to García-Sánchez et al. (2013), the breakthrough curve shows the loading behavior of fluoride ions onto bone char in a fixed bed, which is usually expressed in terms of adsorbed fluoride concentration or relative concentration (C/C_0) as a function of time or volume of effluent for a given bed height, where C_0 is the initial concentration of fluoride and C is the concentration of fluoride at time t. Fig. 4 shows the breakthrough curve for fluoride sorption by bone char. The breakthrough point corresponding to C/C_0 = 0.15 was adopted concerning the limit recommended by the WHO (1.5 mg/L).

The fluoride breakthrough curve presents an asymmetrical S-shape, slowly approaching to $C/C_0 \approx 0.9$, which is a common characteristic of sorption processes in a liquid phase where the pore diffusion phenomena is controlled by the mass transport process

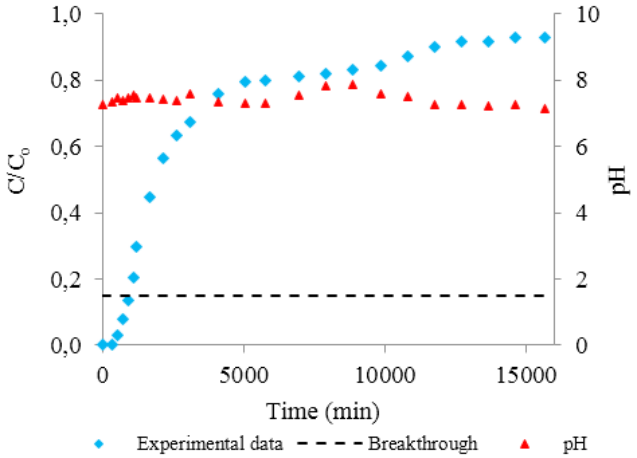

Figure 4. Breakthrough curve of fluoride removal by bone char in a continuous system. Column configuration: Bone char mass: 30.36 g; Bed volume: 54.01 cm^3; Bed height 13 cm; Flow rate 5 mL/min; Temperature: 25ºC; Fluoride initial concentration: (10±0.15) mg/L.

(Aksu and Gonen, 2006; Tovar-Gómez et al. 2013, Nigri et al. 2017a). This behavior has been observed in other studies using several sorbents (García-Sánchez et al. 2013, 2014; Rojas-Mayorga et al. 2015; Tovar-Gómez et al. 2013; Nigri et al. 2017a).

The area under the breakthrough curve represents the total amount of fluoride removed from the feed solution (Kundu and Gupta, 2007; Lodeiro et al., 2006; Nur et al., 2014; Rojas-Mayorga et al., 2015). It is represented through equation (4).

$$q_{tot} = \frac{Q}{1000} \int_{t=0}^{t=tot} C_{ad}\,dt \quad (4)$$

where q_{tot} is the total amount of fluoride sorbed (mg/g), C_{ad} is the difference between initial and equilibrium concentration of fluoride (mg/L), t is time and Q is the feed flow rate (L/min). The fluoride sorption capacity q (mg/g) of bone char can also be determined by equation (5) where M is the sorbent mass (g).

$$q = \frac{q_{tot}}{M} \quad (5)$$

The length of the mass transfer zone - L_{MTZ}, a parameter frequently used to determine the effective height of the sorption column, is defined as the length of the ion exchange zone in the column and can be calculated by equation (6):

$$L_{MTZ} = L\left(\frac{t_e - t_{bt}}{t_e}\right) \quad (6)$$

where L is the bed length (cm), t_{bt} is the breakthrough time (min or h) and t_e is the column exhaustion time. Typically, the breakthrough point is determined when the effluent concentration reaches 5% of the feed concentration, while the exhaustion point is reached when the effluent concentration is equal to 95% of the feed concentration (Nigri et al. 2017a). Table 3 shows the adsorption capacities at the breakthrough time for the relative concentrations C/C_0 = 0.15 and C/C_0 = 0.90 and the length of the mass transfer zone (L_{MTZ}).

Table 3. Adsorption capacities at the breakthrough time at $C/C_0 = 0.15$ and $C/C_0 = 0.90$ for column feed flow rate of 5 mL/min and length of mass transfer zone.

Relative concentration (C/C_0)	Breakthrough time (min)	Sorbed fluoride (mg/g)	L_{MTZ} (cm)
0.15	943.64	1.47	10.06
0.90	14640.00	6.28	

Column configuration: Bone char mass: 30.36 g; Bed volume: 54.01 cm^3; Bed height: 13 cm; Flow rate: 5 mL/min; Temperature: 25ºC; Fluoride initial concentration: (10±0.15) mg/L.

An operation time of 944 min (15.7 h) was obtained at $C/C_0 = 0.15$ and 14640 min (244 h) at $C/C_0 = 0.90$. The adsorption capacity estimated by the area under the breakthrough curve, using *OriginPro8,* indicates loads of 1.47 mg/g and 6.28 mg/g at $C/C_0 = 0.15$ and $C/C_0 = 0.90$, respectively. The adsorption capacity for $C/C_0 = 0.90$ is very similar to the value obtained by Nigri et al. (2017a), who obtained a value of 5.96 mg/g. The length of the mass transfer zone was 10.6 cm using a bed depth of 13 cm. This non-used bed fraction may indicate the existence of preferential paths inside the column and/or high intraparticle resistance.

Adsorption models

A successful adsorption column project requires the prediction of the profile evolution curve for the treated solution (Yan et al., 2001). Several mathematical models have been developed to describe and predict the dynamics of the continuous adsorption process (Aksu and Gonen, 2004). The main applied models are described in the followings sections.

Thomas' model is one of the most applied models for a continuous system. The adsorption capacity is determined considering that the diffusion resistance in the liquid film around the adsorbent particles controls the adsorption and the axial dispersion may be neglected (Aksu and Gonen, 2004; García-Sánchez et al., 2013; García-Sánchez et al., 2014; Ghosh et al., 2015; Thomas, 1944). This model can be seen below in both non-linear (eq.7) and linear forms (eq.8).

$$\frac{C}{C_o} = \frac{1}{1 + e^{\left[\frac{k_t . q_t . M}{Q} - k_t . C_0 . t\right]}} \tag{7}$$

$$\ln\left[\frac{C_o}{C} - 1\right] = \frac{k_t q_t M}{Q} - k_t C_o t \tag{8}$$

In this model k_t is the Thomas constant (L/min.mg), q_t is the adsorption capacity (mg/g), Q is the feed flow rate to the column (mL/min), M is the adsorbent mass (g), C_0 is the feed concentration of adsorbate and C is the concentration of the column effluent at the time t (min), both expressed in mg/L. Those constants (k_t and q_t) are determined from a plot of $\ln[(C_o/C) - 1]$ versus time at a known feed flow rate.

The Yoon-Nelson model (eq. 9) is one of the simplest models for column applications. It does not require any information about the system characteristics such as type of adsorbent and physical properties of the adsorption bed (Samoraj et al., 2016; Yoon and James, 1984). Additionally, the Yoon-Nelson model is extremely concise in form, supposing that the decrease in the probability of each adsorbate to be adsorbed is proportional to the probability of its adsorption and breakthrough on the adsorbent (Xu et al., 2013; Yoon and James, 1984).

$$\frac{C}{C_o} = \frac{e^{(k_{YN} . t - \tau . k_{YN})}}{1 + e^{(k_{YN} . t - \tau . k_{YN})}} \tag{9}$$

The linear form of the Yoon-Nelson model is expressed by equation 10. In addition, Yoon-Nelson and Thomas' models also share some similarities that could result in comparable correlation coefficient, R^2, values (Lau et al., 2016).

$$\ln\left[\frac{C}{C_0 - C}\right] = k_{YN} . t - \tau . k_{YN} \tag{10}$$

where C_0 is the initial solution concentration (mg/L), C is the concentration of the solution at time t (mg/L), τ is the time required for 50% adsorbate breakthrough (min), k_{YN} is the rate constant (1/min) and t (min).

Adams-Bohart's model (eq. 11 and eq.12) has its significance recognized due to its simplicity. This model assumes that the chemical reaction of adsorbate on the adsorbent surface controls the kinetic process, both solute diffusion into the porous layer and volume diffusion being negligible (Lodeiro et al., 2006). However, this model is better applied to describe an initial breakthrough curve limited to $C < 0.5C_0$ since the adsorption rate is proportional to the adsorbed fraction (Bohart and Adams, 1920; Ghosh et al., 2015; Han et al., 2009).

$$\frac{C}{C_o} = e^{\left(k_{AB} C_o t - k_{AB} N_o \frac{Z}{V}\right)} \tag{11}$$

$$\ln\left[\frac{C}{C_0}\right] = k_{AB} C_o t - k_{AB} N_o \frac{Z}{V} \tag{12}$$

In these equations, k_{AB} is the kinetic constant (L/min.mg), V is the linear flow rate (cm/min), Z is the bed height (cm) and N_0 is the saturation concentration (mg/L). Model constants (k_{AB} and N_0) are found from a plot of $\ln[C/C_o]$ versus time.

Based on the results, Wolborska (1989) developed a model to describe the breakthrough in the low concentration region. They observed that the initial segment of the breakthrough curve is controlled by film diffusion with constant kinetic coefficient, the concentration profile of the initial stage moves axially in the column at a constant velocity, and the width of the concentration profile in the column and the final breakthrough curve were nearly constant (Xu et al., 2013). The expression of the Wolborska model (eq. 13 and eq.14) solution is equivalent to the Adams-Bohart relation if the coefficient k_{AB} is equal to β_a/N_o. This equation can also be linearized to give a relationship between $\ln[C/C_o]$ and time from which the model parameters can be calculated (Ushakumary and Madhu, 2014).

$$\frac{C}{C_o} = e^{\left[\left(\frac{\beta_a . C_0}{N_0}\right).t - \left(\frac{\beta_a . H}{v}\right)\right]} \tag{13}$$

$$\ln\left[\frac{C}{C_0}\right] = \left(\frac{\beta_a . C_0}{N_0}\right).t - \left(\frac{\beta_a . H}{v}\right) \tag{14}$$

where C_0 is initial solution concentration (mg/L), C is the concentration of the column effluent at the time t (min), N_0 is the saturation concentration (mg/L), β_a is a kinetic coefficient of the external mass transfer (1/min), H is the bed depth (cm), ν is the migration rate of the solute through the fixed bed (cm/min).

Yan et al. (2001) proposed modifications in the Adams-Bohart model to minimize fitted error, especially at the beginning and the end of the curve. Eqs. 15 and 16 represents the new model and the adsorption capacity at the equilibrium can be obtained from eq. 17 (Yan et al., 2001; Zou et al., 2013).

$$\log\left[\frac{C}{C_0 - C}\right] = a.\log\left(\frac{Q_t}{b}\right) + a.\log\ t \tag{15}$$

$$\frac{C}{C_0} = 1 - \left(\frac{1}{1 + \left(\frac{Q_t}{b}\right)^a}\right) \tag{16}$$

$$q_0 = \frac{b.\ C_0}{M} \tag{17}$$

C_0 being the feed adsorbate concentration, C the adsorbate concentration at time t, both expressed in mg/L, Q_t the throughput volume (L). Parameter b denotes the throughput volume (L) that produces a half-maximum response, a is the slope of the regression function, q_0 represents the adsorption capacity at equilibrium and M is the adsorbent mass.

Fig. 5 shows Thomas, Yoon-Nelson, Adams-Bohart, Wolborska and Yan's models fitted to column experimental data for fluoride removal by bone char. Table 4 presents the modeling parameters obtained through linear and non-linear fitting. The better fit was found from Yan's model with a correlation factor of 0.94 and 0.98, for linear and non-linear curves, respectively. The adsorption capacities determined from this model (4.26 mg/g - linear and 3.60 mg/g - non-linear).

Thomas and Yoon-Nelson model fittings presented lower correlation coefficients ($R^2 < 0.9$);

Table 4. Thomas, Yoon-Nelson, Adams-Bohart, Wolborska and Yan's models parameters for the breakthrough curves of fluoride ions by bone char.

Thomas model	**k_t (mL/mg.min)**	**Standard Error**	**q_0 (mg/g)**	**Standard Error**	**Adj. R-Square**	**Standard Error**
Linear	3.09E-05		6.48		0.71	3.3E-01
Non-linear	9.44E-05	1.75E-05	3.94	0.36	0.88	
Yoon-Nelson	**k_{yn} (1/min)**	**Standard Error**	**τ (min)**	**Standard Error**	**Adj. R-Square**	**Standard Error**
Linear	3.05E-04		3994		0.71	3.3E-01
Non-linear	9.31E-04	1.72E-04	2427	218	0.88	
Adams- Bohart	**k_{AB} (mL/mg.min)**	**Standard Error**	**N_0 (mg/L)**	**Standard Error**	**Adj. R-Square**	**Standard Error**
Linear	1.36E-05		10355		0.44	2.5E-01
Non-linear	8.10E-06	1.59E-06	11986	1	0.59	
Wolborska	**β_a (1/min)**	**Standard Error**	**N_0 (mg/L)**	**Standard Error**	**Adj. R-Square**	**Standard Error**
Linear	0.14		10355		0.44	2.5E-01
Non-linear	0.10	0.02	12103	1096	0.59	
Yan model	**b (L)**	**Standard Error**	**q_0 (mg/g)**	**Standard Error**	**Adj. R-Square**	**Standard Error**
Linear	13.11		4.26		0.94	3.9E-01
Non-linear	11.09	0.52	3.60	0.62	0.98	

Column configuration: Bone char mass: 30.36 g; Bed volume: 54.01 cm^3; Bed height: 13 cm; Flow rate: 5 mL/min; Temperature: 25ºC Fluoride initial concentration: (10±0.15) mg/L.

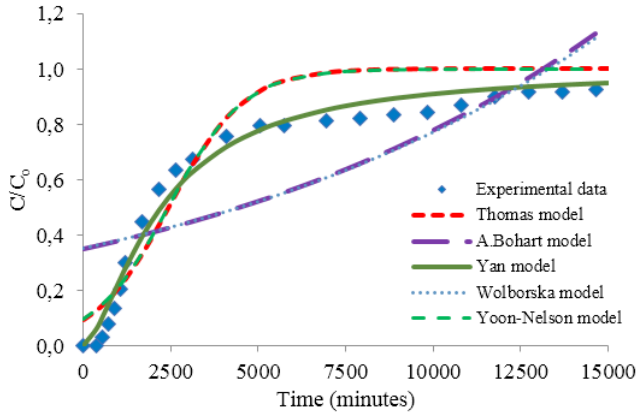

Figure 5. Fit of the Thomas, Yoon-Nelson, Adams-Bohart, Wolborska and Yan's models to breakthrough curve of fluoride ion removal by bone char. Column configuration: Bone char mass: 30.36 g; Bed volume: 54.01 cm^3; Bed height: 13 cm; Flow rate: 5 mL/min; Temperature: 25ºC Fluoride initial concentration: (10±0.15) mg/L.

however, the adsorption capacity of non-linear fitting (3.94 mg/L) is of the same order of Yan's model fit. On the other hand, the Adams-Bohart and Wolborska models do not fit the data since the correlation coefficients are 0.44 and 0.59 for linear and non-linear fitting.

These observations suggest that there is not just one mechanism controlling the adsorption in a fixed bed system. Essentially, the mechanism for fluoride removal, which is in accordance with the proposal of Sternitzke et al. (2012), comprises three main possibilities: fluoride adsorption in calcium sites, substitution of OH^- by F^- and also precipitation of fluorapatite and calcium fluoride. These associated mechanisms govern the fluoride removal and explain the fact that only one model is not able to represent the process, reflected by the observed results.

Error analysis

Error analysis was used to evaluate the models employed in the present study. The error of estimation is given by equation 18.

$$E = \frac{1}{N}\Sigma\left[\left(\frac{C}{C_0}\right)_m - \left(\frac{C}{C_0}\right)_e\right]^2 \quad (18)$$

where C_0 is the initial solution concentration (mg/L), C is the concentration of the solution at time t (mg/L) obtained from the applied models and from the experiment.

The model of Yan presented the smallest error (0.0024) which confirms the best fit obtained. The models of Thomas and Yoon-Nelson presented the similar errors (0.0128) and, finally, the models of Adams-Bohart and Wolborska presented the biggest error (0.0441) and, consequently, the worst adjustment to the experimental data.

Bone char chemical regeneration

Chemical regeneration of bone char was conducted for five cycles up to the rupture of the breakthrough curve in $C/C_0 = 0.15$ in each experiment (Fig. 6). Table 5 shows the amount of water treated, the adsorption capacity and the time needed to reach the relative concentration of $C/C_0 = 0.15$ in each adsorption cycle. There was an overall reduction of 30% in the adsorption capacity from the first to the last adsorption experiment. Also, the same behavior was observed for treated water volume, which was reduced from 4.515 L to 1.350 L.

It is important to note that the adsorption capacity was reduced mainly from the fourth to the fifth cycle. The chemisorption of fluoride by most sorbents is quite strong and not easily reversible. Therefore, stronger acids and bases, as well as a high time of interaction between sorbent and sorbate, are required for efficient F^- elution (Dey et al. 2004: Loganathan et al. 2013; Nigri et al. 2017a). This fact could explain the low regeneration efficiency obtained, highlighting the

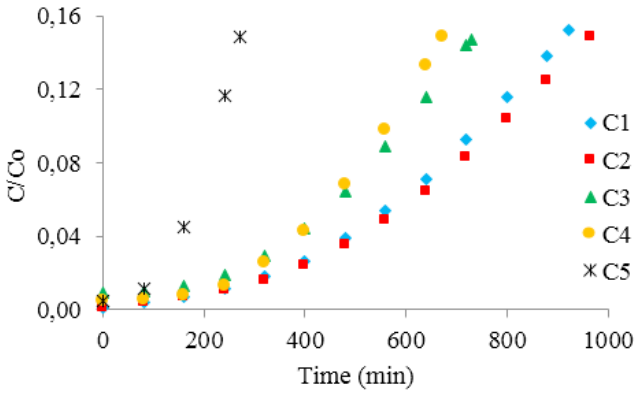

Figure 6. Fluoride breakthrough curves for $C/C_0 = 0.15$ of each adsorption cycle (C). pH(C1): 7.1-8.1; pH(C2): 7.1-8.2; pH(C3): 7.4-8.9; pH(C4): 6.8-7.5; pH(C5): 7.7-8.9. Column configuration: Bone char mass: 30.36 g; Bed volume: 54.01 cm^3; Flow rate 5 mL/min; Temperature: 25ºC; Fluoride initial concentration: (10±0.15) mg/L.

Table 5. Adsorption cycle data of fixed bed breakthrough curves up to $C/C_0 = 0.15$.

Cycle	Breakthrough time (min)	Treated volume (L)	Fluoride adsorption (mg F^-/g bone char)
1	923	4.615	1.42
2	965	4.825	1.52
3	730	3.650	1.16
4	672	3.360	1.07
5	270	1.350	0.43

Column configuration: Bone char mass: 30.36 g; Bed volume: 54.01 cm^3; Flow rate 5 mL/min; Temperature: 25ºC; Fluoride initial concentration: (10±0.15) mg/L; Regeneration solution: NaOH 0.5 mol/L.

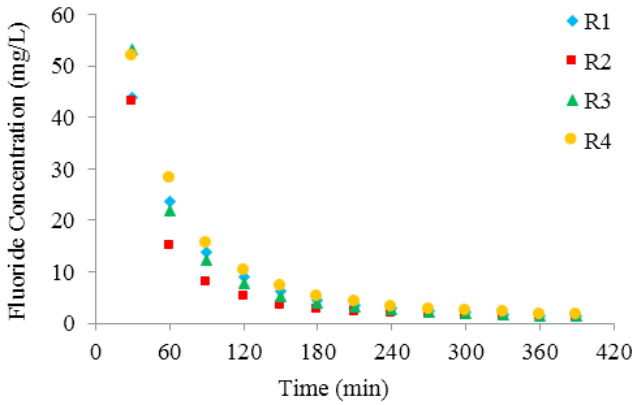

Figure 7. Residual concentration of fluoride in the solution for each regeneration cycle (R). Column configuration: Bone char mass: 30.36 g; Bed volume: 54.01 cm^3; Flow rate: 5 mL/min; Temperature: 25ºC; Regeneration solution: NaOH 0.5 mol/L.

necessity for further studies, possibly using a longer contact time with the sorbent (Nigri et al. 2017a).

Fig. 7 shows the fluoride concentration evolution in chemical regeneration with 0.5 mol/L of NaOH. All cycles of regeneration (R1 to R4) present a high initial fluoride concentration, as observed in the first sample that contains 43-52 mg/L. There is also a pronounced decrease in fluoride concentration until 120 min, indicating a significant fluoride removal through sodium hydroxide solution elution in the first few minutes of desorption.

CONCLUSIONS

Chemical regeneration of bone char in a fixed bed and continuous flow with 0.5 mol/L sodium hydroxide solution is technically feasible during 4 cycles. After the fourth regeneration cycle bone char sorption capacity decreased by 30%, which indicates the need to replace the sorbent in the process.

Adsorption behavior of fluoride ions by bone char (particle size between 1.0-1.6mm) in fixed bed was modeled by Thomas, Adams-Bohart, Yoon-Nelson, Wolborska and Yan's models, the last one being the best fit to the curve with an S shape. The experimental results demonstrated a better fit by Yan's model and the adsorption capacity of 6.28 mg/g was obtained from the breakthrough curve. These results are useful for designing a real defluoridation system.

NOMENCLATURE

a	Slope of the regression function
b	Throughput volume (L)
β_a	Kinetic coefficient of the external mass transfer (1/min)
C_{ad}	Difference between initial and equilibrium concentration of fluoride (mg/L)
C	Concentration of the column effluent in the time t (L/min)
C_0	Feed concentration of adsorbate (L/min)
H	Bed depth (cm)
HAP	Hydroxyapatite
k_{AB}	Kinetic constant (L/min.mg)
k_t	Thomas constant (L/min.mg)
k_{YN}	Rate constant (1/min)
L	Bed length (cm)
L_{MTZ}	Length of mass transfer zone (cm)
M	Adsorbent mass (g)
N_0	Saturation concentration (mg/L)
pH_{PZC}	pH of zero charge point
Q	Feed flow rate to the column (mL/min)
Q_t	Throughput volume (L)
q_t	Adsorption capacity (mg/g)
q_0	Adsorption capacity at equilibrium time
q_{tot}	Total amount of fluoride sorbed (mg/g)
t	Time (min)
t_{bt}	Breakthrough time (min)
t_e	Column exhaustion time (min)
τ	Time required for 50% adsorbate breakthrough (min)
V	Linear flow rate (cm/min)
ν	Migration rate of the solute through the fixed bed (cm/min)
Z	Bed height (cm)

ACKNOWLEDGEMENTS

The authors acknowledge financial support from the Brazilian research funding agencies CAPES (finance code 001) for the pos-doctoral scholarship, CNPq (Process number 311348/2014-9) and FAPEMIG. The authors are also thankful to Bonechar Carvão Ativado do Brasil to the bone char supply.

REFERENCES

Abe, I., Iwasaki, S., Tokimoto, T., Kawasaki, N., Nakamura, T., Tanada, S. Adsorption of fluoride ions onto carbonaceous materials. J. Colloid. Interface Sci., 275, 35-39 (2004). https://doi.org/10.1016/j.jcis.2003.12.031

Agarwal, M., Rai, K., Shrivastav, R., Dass, S. Defluoridation of water using amended clay. J. Clean. Prod., 11, 439-444 (2003). https://doi.org/10.1016/S0959-6526(02)00065-3

Aksu, Z., Gonen, F. Biosorption of phenol by immobilized activated sludge in a continuous packed bed: prediction of breakthrough curves. Process Biochem., 39, 599-613 (2004). https://doi.org/10.1016/S0032-9592(03)00132-8

Aksu, Z., Gonen, F. Binary biosorption of phenol and chromium(VI) onto immobilized activated sludge in a packed bed: prediction of kinetic parameters

and breakthrough curves. Sep. Purif. Technol., 49, 205-216 (2006). https://doi.org/10.1016/j.seppur.2005.09.014

APHA - American Public Health Association. Standard methods for the examination of water and wastewater. 22nd ed. Washington (2012).

Benefield, L. D., Junking, J. F., Weand, B. L. Process Chemistry for Water and Wastewater Treatment. Prentice Hall, Upper Saddle River, NJ, pp. 405-421 (1982).

Bhatnagar, A., Kumar, E., Sillanpaa, M. Fluoride removal from water by adsorption-a review. Chem. Eng. J., 171, 811-840 (2011). https://doi.org/10.1016/j.cej.2011.05.028

Bohart, G., Adams, E. Q. Some aspects of the behavior of charcoal with respect to chlorine, J. Am. Chem. Soc., 42, 523-544 (1920). https://doi.org/10.1021/ja01448a018

Brunson, L. R., Sabatini, D. A. An evaluation of fish bone char as an appropriate arsenic and fluoride removal technology for emerging regions. Environ. Eng. Sci., 26, 1777-1784 (2009). https://doi.org/10.1089/ees.2009.0222

Burwell, R. L. Manual of symbols and terminology for physicochemical quantities and units - appendix 2 - definitions, terminology and symbols in colloid and surface-chemistry. 2. Heterogeneous catalysis. Pure Appl. Chem., 46, 71 (1976). https://doi.org/10.1016/B978-0-08-021360-6.50005-X

Colla, V., Branca, T. A., Rosito, F., Lucca, C., Vivas, B. P., Delmiro, V. M. Sustainable reverse osmosis application for wastewater treatment in the steel industry. J. Clean. Prod., 130, 103-115 (2016). https://doi.org/10.1016/j.jclepro.2015.09.025

Cheung, C. W., Porter, J. F., McKay, G. Removal of Cu(II) and Zn(II) ions by sorption onto bone char using batch agitation. Langmuir, 18, 650-656 (2002). https://doi.org/10.1021/la010706m

Davila-Rodriguez, J. L., Escobar-Barrios, V. A., Rangel-Mendez, J. R. Removal of fluoride from drinking water by a chitin-based biocomposite in fixed-bed columns. J. Fluorine Chem., 140, 99-103 (2012). https://doi.org/10.1016/j.jfluchem.2012.05.019

Dey, S., Goswami, S., Ghosh, U. C. Hydrous ferric oxide (HFO)-a scavenger for fluoride from contaminated water. Water Air Soil. Pollut., 158, 311-323 (2004). https://doi.org/10.1023/B:WATE.0000044854.71497.b6

Dimović, S., Smičiklas, I., Plećaš, I., Antonović, D., Mitrić, M. Comparative study of differently treated animal bones for CO^{2+} removal. J. Hazard. Mater., 164, 279-287 (2009). https://doi.org/10.1016/j.jhazmat.2008.08.013

Feng, L., Xu, W., Liu, T., Liu, J. Heat regeneration of hydroxyapatite/attapulgite composite beads for defluoridation of drinking water. J. Hazard. Mater., 221, 228-235 (2012). https://doi.org/10.1016/j.jhazmat.2012.04.040

García-Sánchez, J. J., Solache-Rios, M., Martinez-Miranda, V., Morelos, C. S., Removal of fluoride ions from drinking water and fluoride solutions by aluminum modified iron oxides in a column system. J. Colloid. Interface Sci., 407, 410-415 (2013). https://doi.org/10.1016/j.jcis.2013.06.031

García-Sánchez, J. J., Solache-Ríos, M., Alarcón-Herrera, M. T., MartínezMiranda, V. Removal of fluoride from well water by modified iron oxides in a column system. Desalin. Water Treat., 57, 2125-2133 (2014). https://doi.org/10.1080/19443994.2014.980332

Ghorai, S., Pant, K. K. Investigations on the column performance of fluoride adsorption by activated alumina in a fixed-bed. Chem. Eng. J., 98, 165-173 (2004). https://doi.org/10.1016/j.cej.2003.07.003

Ghosh, A., Chakrabarti, S., Biswas, K., Ghosh, U. C. Column performances on fluoride removal by agglomerated Ce(IV)-Zr (IV) mixed oxide nanoparticles packed fixed-beds. J. Environ. Chem. Eng., 3, 653-661 (2015). https://doi.org/10.1016/j.jece.2015.02.001

Gupta, V. K., Ali, I., Saino, V. K. Defluoridation of wastewaters using waste carbon slurry. Water Res., 41, 3307-3316 (2007). https://doi.org/10.1016/j.watres.2007.04.029

Gwala, P., Andey, S., Mhaisalkar, V., Labhasetwar, S., Kshirsagar, C. Lab scale study on electrocoagulation defluoridation process optimization along with aluminium leaching in the process and comparison with full-scale plant operation. Water Sci. Technol., 63, 2788-2795 (2011). https://doi.org/10.2166/wst.2011.475

Han, R., Zou, L., Zhao, X., Xu, Y., Xu, F., Li, Y., Wang, Y. Characterization and properties of iron oxide-coated zeolite as adsorbent for removal of copper (II) from solution in fixed bed column. Chem. Eng., 149, 123-131 (2009). https://doi.org/10.1016/j.cej.2008.10.015

Harrison, P. T. C. Fluoride in water: a UK perspective. J. Fluorine Chem., 126, 1448-1456 (2005). https://doi.org/10.1016/j.jfluchem.2005.09.009

Jacobsen, P. Mueller, K. CDN's Experiences inProducing Bone Char. (2007). Viewed September 2017, <https://www.eawag.ch/fileadmin/Domain1/Forschung/Menschen/Trinkwasser/Wrq/bone_char_production.pdf>.

Kanyora, A. K., Kinyanjui, T. K., Kariuki, S. M., Chepkwony, C. K. Efficiency of various sodium solutions in regeneration of fluoride saturated bone char for de-fluoridation. IOSR J Environ Sci. Toxicol. Food Technol., 8, 10-16 (2014). https://doi.org/10.9790/2402-081031016

Kanyora, A., Kinyanjui, T., Kariuki, S., Njogu, M. Fluoride removal capacity of regenerated bone char in treatment of drinking water. Asian J. Nat. Appl. Sci., 4, 30-36 (2015).

Kaseva, M. E. Optimization of regenerated bone char for fluoride removal in drinking water: a case study in Tanzania. J. Water Health, 4, 139-147 (2006). https://doi.org/10.2166/wh.2006.0011

Krzesińska, M., Majewska, J. Physical properties of continuous matrix of porous natural hydroxyapatite related to the pyrolysis temperature of animal bones precursors. J. Anal. Appl. Pyrolysis, 116, 202-214 (2015). https://doi.org/10.1016/j.jaap.2015.09.009

Kunin, R. Ion Exchange Resins. Krieger, R. E. Publishing Co, Florida, pp. 135-139 (1990).

Kundu, S., Gupta, A. K. As(III) removal from aqueous medium in fixed bed using iron oxide-coated cement (IOCC): Experimental and modeling studies. Chem. Eng. J., 129, 123-131 (2007). https://doi.org/10.1016/j.cej.2006.10.014

Lau, L. C., Nor, N. M., Lee, K. T., Mohamed, A. R. Adsorption isotherm, kinetic, thermodynamic and breakthrough curve models of H_2S removal using CeO_2/NaOH/PSAC. Int J Petrochem. Sci. Eng., 1, 36-44 (2016). https://doi.org/10.15406/ipcse.2016.01.00009

Leyva-Ramos, R., Rivera-Utrilla, J., Medellin-Castillo, N. A., Sanchez-Polo, M. Kinetic modelling of fluoride adsorption from aqueous solution onto bone char. Chem. Eng. J., 158, 458-467 (2010). https://doi.org/10.1016/j.cej.2010.01.019

Lodeiro, P., Herrero, R., Vicente, M. E. S. The use of protonated Sargassum muticum as biosorbent for cadmium removal in a fixed-bed column. J. Hazard. Mater., 137, 244-253 (2006). https://doi.org/10.1016/j.jhazmat.2006.01.061

Loganathan, P., Vigneswaran, S., Kandasamy, J., Naidu, R. Defluoridation of drinking water using adsorption processes. J. Hazard. Mater., 248-249, 1-19 (2013). https://doi.org/10.1016/j.jhazmat.2012.12.043

Medellin-Castillo, N. A., Leyva-Ramos, R., Ocampo-Perez, R., de la Cruz R. F. G., Aragon-Pina, A., Martinez-Rosales, J. M., Guerrero-Coronado, R. M., Fuentes-Rubio, L. Adsorption of fluoride from water solution on bone char. Ind. Eng. Chem. Res., 46, 9205-9212 (2007). https://doi.org/10.1021/ie070023n

Medellin-Castillo, N. A., Leyva-Ramos, R., Padilla-Ortega, E., Perez, R. O., Flores-Cano, J. V., Berber-Mendoza, M. S. Adsorption capacity of bone char for removing fluoride from water solution. Role of hydroxyapatite content, adsorption mechanism and competing anions. J. Ind. Eng. Chem., 20, 4014-4021 (2014). https://doi.org/10.1016/j.jiec.2013.12.105

Meneasse, L. N., Fantinel, L. M., Knauer, L. G., Horn, A. H., Dupont, H. S. J. B., Castro, R. E. L., Freira, A. P. S., Efigênia, F., Paixão, H. H., Castilho, L., Bazzoli, N., Santos, C. V. N., Souza, C. A. S., Lúcio, P. S., Flúor na água subterrânea e fluorose dental no município de São Francisco, Minas Gerais. In: Congresso Brasileiro de Geologia, 41, João Pessoa, Anais, p. 554 (2002).

Samoraj, M., Tuhy, L., Rusek, P., Rój, E., Chojnacka, K. Pilot Plant Conversion of Blackcurrant Seeds into New Micronutrient Fertilizer Biocomponents via Biosorption. BioResources, 11, 400-413 (2016). https://doi.org/10.15376/biores.11.1.400-413

Nasr, B., Walha, K., Charcosset, C., Bem Amar, R. Removal of fluoride ions using cuttlefish bones. J. Fluor. Chem., 132, 57-62 (2011). https://doi.org/10.1016/j.jfluchem.2010.11.006

Nigri, E. M., Cechinel, M. A. P., Mayer, D. A., Mazur, L. P., Loureiro, J. M., Rocha, S. D. F., Vilar, V. J. P. Cow bones char as a green sorbent for fluorides removal from aqueous solutions: batch and fixed-bed studies. Environ. Sci. Pollut. Res., 24, 2364-2380 (2017a). https://doi.org/10.1007/s11356-016-7816-5

Nigri, E. M., Bhatnagar, A., Rocha, S. D. F. Thermal regeneration process of bone char used in the fluoride removal from aqueous solution. J. Clean. Prod., 142, 3558-3570 (2017b). https://doi.org/10.1016/j.jclepro.2016.10.112

Nur, T., Loganathan, P., Nguyen, T. C., Vigneswaran, S., Singh, G., Kandasamy, J. Batch and column adsorption and desorption of fluoride using hydrous ferric oxide: solution chemistry and modeling. Chem. Eng. J., 247, 93-102 (2014). https://doi.org/10.1016/j.cej.2014.03.009

Rojas-Mayorga, C, K., Bonilla-Petriciolet, A., Aguayo-Villarreal, I. A., Hernandez-Montoya, V., Moreno-Virgen, M. R., Tovar-Gomez, R., Montes-Moran, M. A. Optimization of pyrolysis conditions and adsorption properties of bone char for fluoride removal from water. J. Anal. Appl. Pyrolysis, 104, 10-18 (2013). https://doi.org/10.1016/j.jaap.2013.09.018

Rojas-Mayorga, C. K., Bonilla-Petriciolet, A., Sánchez-Ruiz, F. J., Moreno-Pérez, J., Reynel-Ávila, H. E., Aguayo-Villarreal, I. A., Mendoza-Castillo, D. I. Breakthrough curve modeling of liquid-phase adsorption of fluoride íons on aluminum-doped bone char using micro-columns: effectiveness of data fitting approaches. J. Mol. Liq., 208, 114-121 (2015). https://doi.org/10.1016/j.molliq.2015.04.045

Santiago, M. R., Silva, J. L. S. Flúor em águas subterrâneas: Um problema Social. In: Anais do XVIII Simpósio Brasileiro de Recursos Hídricos. Campo Grande. MS.1-5p (2009).

Sheintuch, M., Matatov-Metal, Y. I. Comparison of catalytic processes with other regeneration methods of activated carbon. Catal. Today, 53, 73-80 (1999). https://doi.org/10.1016/S0920-5861(99)00104-2

Simons, R. Trace element removal from ash dam waters by nanofiltration and diffusion dialysis. Desalination, 89, 325-341 (1993). https://doi.org/10.1016/0011-9164(93)80145-D

Sternitzke, V., Kaegi, R., Audinot, J. N., Lewin, E., Hering, J. G., Johnson, C. A. Uptake of fluoride from aqueous solution on nano-sized hydroxyapatite: examination of a fluoridated surface layer. Environ. Sci. Technol., 46, 802-809 (2012). https://doi.org/10.1021/es202750t

Sundaram, C. S., Viswanathan, N., Meenakshi, S. Defluoridation chemistry of synthetic hydroxyapatite at nano scale: equilibrium and kinetic studies. J. Hazard. Mater, 155, 206-215 (2008). https://doi.org/10.1016/j.jhazmat.2007.11.048

Thomas, H. C. Heterogeneous ion exchange in a flowing system, J. Am. Chem. Soc., 66, 1664-1666 (1944). https://doi.org/10.1021/ja01238a017

Tovar-Gómez, R., Moreno-Virgen, M. R., Dena-Aguilar, J. A., Hernández-Montoya, V., Bonilla-Petriciolet, A., Montes-Morán, M. A. Modeling of fixed-bed adsorption of fluoride on bone char using a hybrid neural network approach. Chem. Eng. J., 228, 1098-1109 (2013). https://doi.org/10.1016/j.cej.2013.05.080

Tripathy, S. S., Bersillon, J. L., Gopal, K. Removal of fluoride from drinking water by adsorption onto alum-impregnated activated alumina. Sep. Purif. Technol., 50, 310-317 (2006). https://doi.org/10.1016/j.seppur.2005.11.036

Thompson, T. J., Gauthier, M., Islam, M. The application of a new method of fourier transform infrared spectroscopy to the analysis of burned bone. J. Archaeol. Sci., 36, 910-914 (2009). https://doi.org/10.1016/j.jas.2008.11.013

Tianyuan, M., Zhiguo, X., Libing, L. Effect of reaction systems and surfactant additives on the morphology evolution of hydroxyapatite nanorods obtained via a hydrothermal route. Appl. Surf. Sci., 257, 4384-4388 (2011). https://doi.org/10.1016/j.apsusc.2010.12.067

Ushakumary, E. R., Madhu, G. Studies on Zinc (II) Adsorption Using Alisma Plantago Aquatica. J. Clean. Energy Technol., 2, 112-117 (2014). https://doi.org/10.7763/JOCET.2014.V2.103

Vocciante, M., Trofa, M., Rodríguez-Estupiñãn, P., Giraldo, L., D'Auria, T., Moreno-Piraján, J. C., Erto, A. A rigorous procedure for the design of adsorption units for the removal of cadmium and nickel from process wastewaters. J. Clean. Prod., 77, 35-46 (2014). https://doi.org/10.1016/j.jclepro.2013.12.001

Walker, G. M., Weatherley, L. R. Adsorption of dyes from aqueous solution - the effect of adsorbent pore size distribution and dye aggregation. Chem. Eng. J., 83, 201-206 (2001). https://doi.org/10.1016/S1385-8947(00)00257-6

Wilson, J. A., Pulford, I. D., Thomas, S. Sorption of Cu and Zn by bone charcoal. Environ. Geochem. Health, 25, 51-56 (2003). https://doi.org/10.1023/A:1021288529358

Wolborska, A. Adsorption on activated carbon of p-nitrophenol from aqueous solution. Water Research, 23, 85-91 (1989). https://doi.org/10.1016/0043-1354(89)90066-3

World Health Organization (WHO), Health Criteria and Other Supporting Information. Guidelines for Drinking-water Quality, second ed., vol. 2. World Health Organization, Geneva (1996).

Xiong, X., Liu, J., He, W., Xia, T., He, P., Chen, X., Yang, K., Wang, A. Dose-effect relationship between drinking water fluoride levels and damage to liver and kidney functions in children, Environ. Res., 103, 112-116 (2007). https://doi.org/10.1016/j.envres.2006.05.008

Xu, Z., Cai, J., Pan, B. Review: Mathematically modeling fixed-bed adsorption in aqueous systems. Appl. Phys. & Eng., 14, 155-176 (2013). https://doi.org/10.1631/jzus.A1300029

Yan, G., Viraraghavan, T., Chen, M. A new model for heavy metal removal in a biosorption column. Adsorpt. Sci. Technol., 19, 25-43 (2001). https://doi.org/10.1260/0263617011493953

Yoon, Y. H., James, H. N. Application of gas adsorption kinetics I. A theoretical model for respirator cartridge service life. Am. Ind. Hyg. Assoc. J., 45, 509-516 (1984). https://doi.org/10.1080/15298668491400197

Zou, W., Zhao, L., Zhu, L. Adsorption of uranium (VI) by grape fruit peel in a fixed bed column: experiments and prediction of breakthrough curves. J. Radioanal. Nucl. Chem., 295, 717-727 (2013). https://doi.org/10.1007/s10967-012-1950-4